4

Radio Observations of GRB030329 Afterglow

4.1 The Gamma Ray Burst of 29th March 2003

The Gamma Ray Burst of 29th March 2003 has been an unique event. At a distance of $\sim$ 870 Mpc (assuming a cosmology of $\Omega_\Lambda = 0.7$ and $\Omega_m = 0.3$, and a redshift of 0.1685 [62]), it is one of the nearest GRB for which an afterglow has been observed. The optical and radio afterglow of this burst has been one of the brightest detected till date [102]. The spectral signature of a supernova (SN2003dh) emerged in the optical transient a few days after the burst [129] and thus provided the first unambiguous evidence of the long suspected association between Gamma Ray Bursts and Supernovae.

GRB030329 was detected and localized by the HETE-II satellite [136]. The trigger H2652 occurred on 29th March 2003, at UT 11:37:14.7 and lasted more than 100 s. This was one of the brightest bursts detected by the instrument, with a $30 - 400$ KeV fluence of 1.1×10^{-4} erg cm^{-2}. The Soft X-ray Camera on board HETE - II localized the burst to be at RA (J2000) = $10^{\rm h}44^{\rm m}49^{\rm s}$ and Dec (J2000) = $+21^\circ 28' 44''$ within an error circle of radius 2 arcmin. Fluence in the lower energy band, $S_{(7-30{\rm KeV})}$, was 5.5×10^{-5}erg cm^{-2}, which implies a hardness ratio, $S_{(7-30{\rm KeV})}/S_{(30-400{\rm KeV})} > 0.33$, classifying this GRB into the 'X-ray rich' category

[138]. In a worldwide observational campaign, the afterglow was detected in all possible wavebands. The first X-ray detection by *RXTE*, around hours after the burst found the source to be extremely bright with a $2-10$ KeV flux of 1.4×10^{-10} erg cm^{-2} sec^{-1} [87]. The optical transient had an R-band magnitude ~ 12 when it was reported by Peterson & Price [102] and Torii [134]. The VLA detected a bright 3.5 mJy radio afterglow at 8.46 GHz on 2003 March 30.06 UT [13]. The Giant Meterwave Radio Telescope (GMRT) made an 8σ detection of the source at 1.4 GHz on March 31.75 UT [107]. Later follow up observations were reported subsequently [70, 81, 108, 109]. Around 7 days after the burst the optical spectrum showed signature of underlying supernova emission [68, 89, 129] and the presence of the associated supernova SN2003dh was confirmed later by spectroscopic measurements. Continued monitoring has provided an unprecedentedly rich temporal coverage of the transient in all wavebands [11, 85, 123, 132].

4.2 The Importance of Radio Observations

Typical radio afterglow flux is usually not significantly above the sensitivity limit of telescopes operational at present. Hence, only a small fraction of radio afterglows are detected. The statistics upto year 2005 shows $\sim 12\%$ of radio afterglow detections, whereas it is nearly 50% for both optical and x-ray afterglows [From http://www.mpe.mpg.de/~jcg/grbgen.html]. In the synchrotron spectrum of the afterglow, the peak frequency ν_m and the self-absorption frequency ν_a reside in or near the radio band. Hence, the flux decay is slower in radio bands, especially in low radio frequencies (≤ 1 GHz). At a given frequency, the flux will not decrease until either ν_m passes through the band or the initial jet expands laterally. If ν_a is above ν_m, the flux will rise until ν_a crosses the band. Hence, if bright enough, the radio afterglow will remain long lived, even for months or years, giving a rare opportunity to study the late time evolution of the fireball; most importantly, the non-relativistic transition.

Rarely has one been able to detect and monitor radio afterglows, and the late time dynamics of the fireball remains a fairly unexplored regime. The only detailed observation campaign prior to GRB030329 was for GRB970508 by the

VLA, which resulted in a $\sim$ 500 day lightcurve in 8, 4 and 1.4 GHz bands, extending well beyond the non-relativistic transition of the fireball.

Moreover, radio afterglows have shown non-standard features in past. A few afterglows which were detected and followed up for timescales of days, have deviated from the standard model predictions to display a slower evolution than expected [49]. This behaviour is not completely explained, though several suggestions have been made [99].

As mentioned earlier, the radio bands fall near the optically thick regime of the afterglow synchrotron spectrum, for typical parameters. This aspect also makes the waveband special. By continuous monitoring of the radio flux evolution, transition of the fireball from optically thick to optically thin regime can be spotted and hence the value of ν_a can be inferred. Thus, the ambient medium density as well as the size of the fireball can be determined, if the total energy is known.

4.3 GMRT – The Low Frequency Radio Telescope

The Giant Meterwave Radio Telescope is located in the Khodad village of Maharashtra, Western-India. It is an interferometric array of 30 elements, arranged in the shape of a 'Y' (see figure 4.1). There is a 'central square' which consists of 14 antennas, and there are three 'arms', named east, west and south. The maximum baseline achievable is 25 kilometers. The full array provides high angular resolution (1.9" in 1280 MHz). Each GMRT antenna is of 45 m diameter. They are fully steerable parabolic dishes, with several feeds operating at spot frequencies between 50 to 1500 MHz. GMRT has excellent sensitivity in low frequencies. In 1280 MHz and 610 MHz bands, the array has a theoretical rms limit of roughly 20 and 15μJy respectively, with 4 hours integration on source using a bandwidth of 16 MHz. This superb sensitivity helped us detecting the source, even down to a few hundred micro janskies in both the bands.

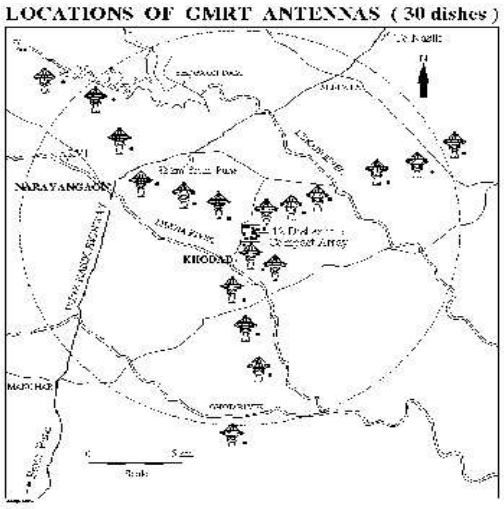

Figure 4.1. Giant Meterwave Radio Telescope, antenna locations.

4.4 GMRT Observations of the Radio Afterglow

The first observation of the afterglow was on 2nd April, 2003, $\sim$ 2 days past the burst [108]. The source was detected in $\sim$ 1280 MHz band with a flux of $330 \pm 90\mu$Jys. The source is being followed up since then once in two to three months in both the frequencies. In this chapter we are presenting the observations done from January to September, 2004 in both 1280 MHz band and in 610 MHz band.

In all the runs, the source was observed for roughly 4 hours. A primary flux calibrator of known flux density (3c286, 3c147 or 3c48), was observed at the beginning and at the end of each observation for 10 to 15 minutes. This was done to convert the visibility amplitude to flux density. The antenna based gain could fluctuate during the course of observation. To correct this, a secondary calibrator (also known as phase calibrator), which is an unresolved source, is used. We observed either 1021+219 or 1125+261 for 5 to 7 minutes in between every 30 to 45 minutes scan on the afterglow, for this purpose.

The data are retrieved in two side bands as `FITS` files. The upper and lower sidebands, each composed of 128 channels of 125 kHz bandwidth, constitute a

total bandwidth of 32 MHz. The data reduction is done offline, using the *Astronomical Image Processing Software* (`AIPS`). The data were edited using the tasks `TVFLG/UVFLG` to remove bad baselines and visibilities. This was done for both polarisations separately. The lower sideband was found corrupted by bad data and we considered only the upper side band for the analysis. Using one representative channel, visibilities of the secondary calibrator were calibrated using the primary calibrator, and the former were then used to calibrate the afterglow visibilities. The bandpass calibration is done by using the task `BPASS` and all good channels (typically channel numbers 15 – 100) were collapsed using the task `SPLAT` to form a single channel dataset. The afterglow visibilities were extracted from this single channel data to form a single source file.

The full resolution maps, at all frequencies, were made using the task `IMAGER`. We used the whole range of visibilities available, and applied a uniform weighting to obtain the best resolution. A few rounds of phase self-calibration and one round of amplitude-self calibration was done to achieve better quality maps. For 610 MHz, polyhedral wide field imaging was done to correct for the effects of non-coplanarity. A few arcminutes of the maps centering the afterglow position (RA=$10^h44^m50^s$, $\delta = 21^\circ31'17"$ [130]), marked by a cross, are displayed in figures 4.2, 4.4 and 4.5. The angular resolution varied between epochs due to dead antennas and bad data.

The flux was estimated using `JMFIT`, by fitting a gaussian of fixed width (that of the synthesised beam size) and solving for the peak intensity and the source position. We present the results in table 4.1. The error quoted along with the flux values represent the 1-σ noise fluctuations in the final image, calculated at an apparent source-free region of the map. The afterglow flux is compared with that of known background sources to check for calibration consistency between the frames. In figures 4.3 and 4.6, the afterglow flux is plotted along with that of a nearby source at RA = $10^h44^m59.473^s$ and $\delta = 21^\circ31'43.89"$.

Mid UT	Flux (mJy)	Mid UT	Flux (mJy)
1280 MHz		610 MHz	
Jun 28.28	0.97 ± 0.14	Feb 26.63	1.15 ± 0.25
Jul 18.31	0.90 ± 0.11	Apr 10.49	0.61 ± 0.11
Aug 20.04	0.90 ± 0.12	Jun 27.28	1.01 ± 0.18
Sep 17.96	0.42 ± 0.09	Jul 20.28	0.84 ± 0.17
		Sep 6.0	0.98 ± 0.15

Table 4.1. The catalog of GMRT observations in 1280 & 610 MHz bands. The last observation in 1280 MHz band gave rise to relatively lower flux value. This could be due to some unknown errors, and we thus neglected this point in fits provided in chapter 5

4.5 Conclusion

The radio afterglow of GRB030329 is still visible at low radio frequencies and has given a unique opportunity for the study of late time evolution of the fireball. We are presenting the observations done till September 2004, in both 1280 MHZ and 610 MHz in this chapter. The model explaining this observations along with those of other wavebands will be described in the next chapter.

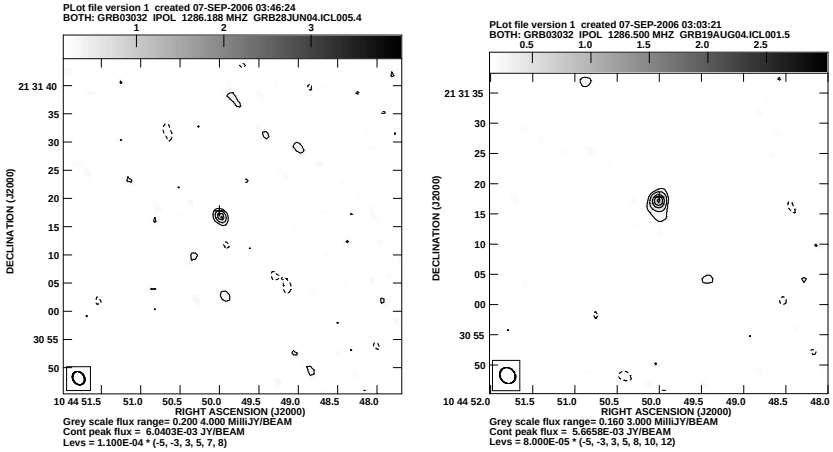

(a) 28th June 2004 **(b)** 20th August 2004

(c) 18th July 2004 **(d)** 17th Sep 2004

Figure 4.2. Field around the afterglow in 1280 MHz. The position of the afterglow is marked by a cross. Equal intensity contours of flux levels in multiplication of the map rms is also plotted along with grayscale.

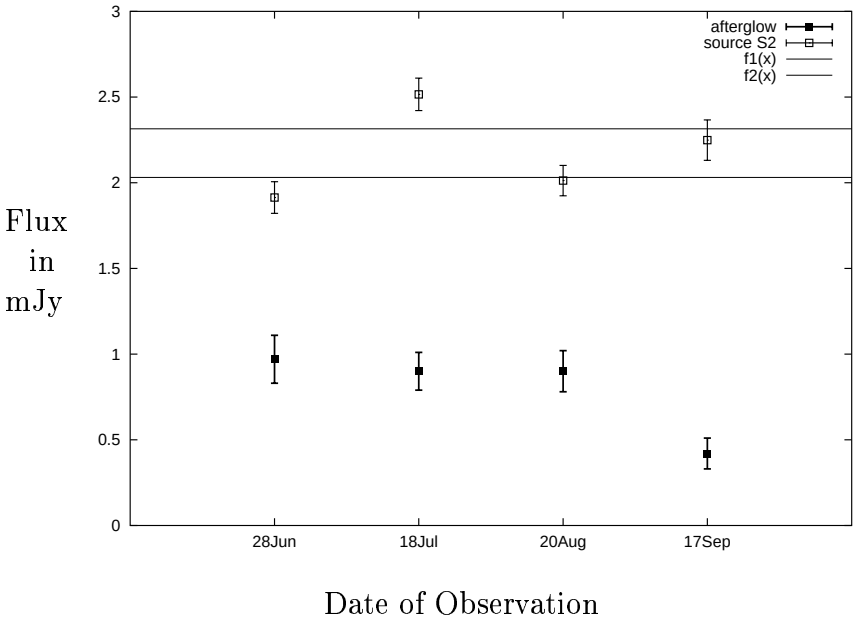

Figure 4.3. 1280 MHz flux of the afterglow along with that of a constant background source. The x-axis shows the date of observations and y-axis the flux estimated for both the sources. The variations in flux appear to be correlated. The mean fluctuation of the background source flux over the four frames presented here is 0.23 mJy. This can be considered as the systematic error in the afterglow flux measurement. The dotted lines show the upper and lower limit of the background source flux from the FIRST survey.

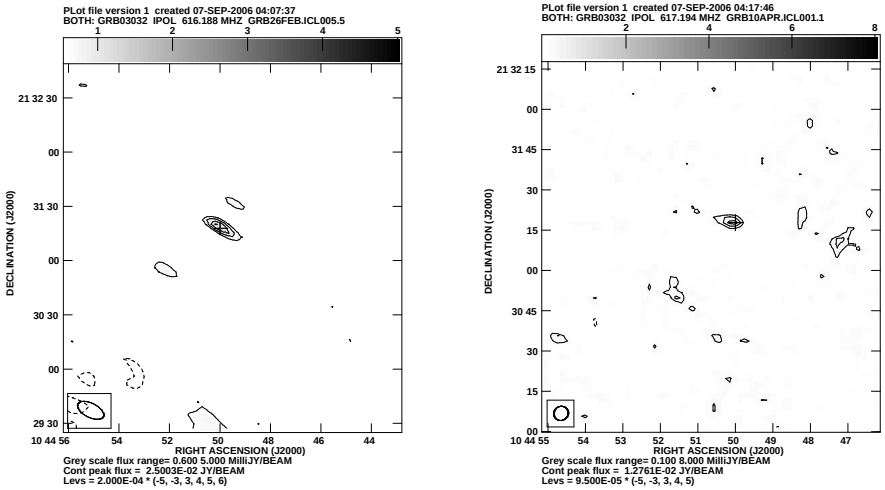

(a) 26th Feb 2004 **(b)** 10th April 2004

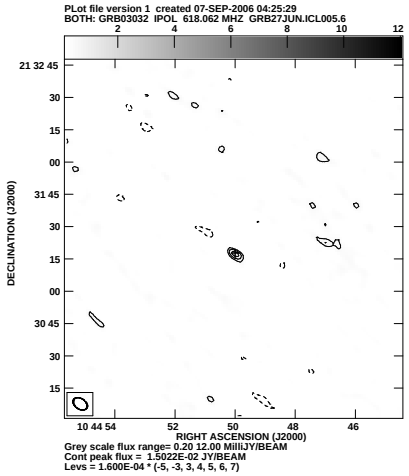

(c) 27th June 2004

Figure 4.4. Field around the afterglow in 610 MHz. The position of the afterglow is marked. Equal intensity contours of flux levels in multiplication of the map rms is also plotted along with the grayscale.

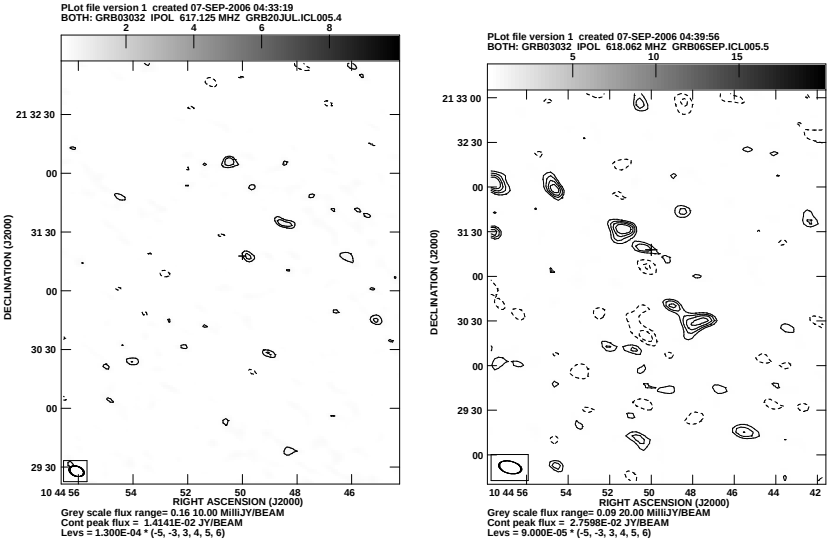

(a) 20th Jul 2004 **(b)** 6th Sep 2004

Figure 4.5. 610 MHz maps (contd.)

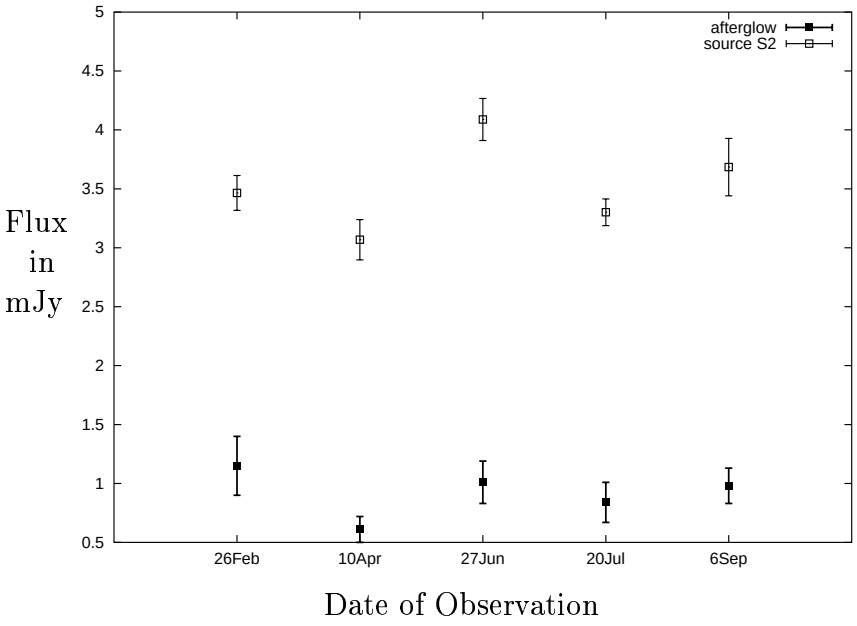

Figure 4.6. 610 MHz flux of the afterglow along with that of the same constant background source as in figure 4.4. The x-axis shows the date of observations and y-axis the flux estimated for both the sources. The variations in flux appear to be correlated. The mean fluctuation of the background source is estimated as 0.35 mJy, and should be considered as the error in the estimate.